

# Ac losses in multifilamentary high- $T_C$ tapes due to a perpendicular ac magnetic field

P Fabricatore<sup>†</sup>, S Farinon<sup>†</sup>, F Gömörý<sup>‡</sup> and S Innocenti<sup>†</sup>

<sup>†</sup> Istituto Nazionale di Fisica Nucleare, Via Dodecaneso, 33-16146 Genova, Italy

<sup>‡</sup> Institute of Electrical Engineering, Slovak Academy of Sciences, Dubravská cesta, 9-84239 Bratislava, Slovak Republic

Received 4 May 2000, in final form 14 June 2000

**Abstract.** Ac losses in mono and multifilamentary high- $T_C$  tapes exposed to a harmonic magnetic field perpendicular to the tape surface are considered. By writing the ac dissipation in terms of the ac magnetic susceptibility, we have two parameters: the imaginary part of the internal ac susceptibility  $\chi''$  and the external susceptibility in the Meissner state  $\chi_0$ , related to the demagnetization. These two terms of the ac loss formula are analysed in detail through both theoretical and experimental approaches. We have used finite-element codes to determine  $\chi_0$  for the three tapes under study, and then we have compared the predictions and the experimental results. Existing theories have been used to calculate  $\chi''$  as a function of the amplitude of the ac magnetic field and have been verified through measurements.

## 1. Introduction

High- $T_C$  superconducting multifilamentary tapes are, for the time being, the most serious candidates for applications in electrical energy transportation. Typical examples are the up-to-date Bi-2223/Ag tapes that contain superconducting material in the form of filaments embedded in a silver matrix. One of the main tasks of the design is to minimize the ac dissipation due to the cyclic variations of the electrical and magnetic fields. This results from the interaction of an electromagnetic field with the two different materials. The currents in a metallic matrix obey Ohm's law, while the characterization of a superconductor should comprise its nonlinear and hysteretic properties. This is why in the losses one can also recognize two contributions. One is due to ohmic dissipation in the metallic matrix and ceases when the frequency of the applied field is decreased. The other is intrinsic for the hard superconductor and also remains finite in the limit of the frequency going to zero. It is this second contribution to the dissipation that we are dealing with in this paper. In this way, the properties of the metallic matrix are identical to those of a vacuum in our calculations. Accordingly, on the experimental side, we choose the frequencies so that they are low enough to observe the frequency independence of the measured properties. We study the case when the sample does not carry any transport current and is exposed to a perpendicular external magnetic field, i.e. that applied in the direction normal to the wide face of the superconducting tape. The difficulty in analysing this problem comes from the large demagnetization due to the high aspect ratio of the tape: the thickness of any superconducting filament in it is much smaller than the width

(the ratio is usually between 10 and 20), and the same is true for the filamentary zone as a whole. As a result we have a large field amplification on both filament and tape edge, and consequently a large ac loss. This can be seen, in a simple way, by introducing the ac susceptibility. In general, the ac dissipation, per unit volume in a harmonic external field  $B = B_0 \cos \omega t$ , can be written as the loop integral of the magnetization,  $M$ , with respect to the applied field:

$$W = \frac{1}{\mu_0} \oint_{\text{cycle}} M dB \quad (1)$$

where  $\mu_0 = 4\pi \times 10^{-7} \text{ H m}^{-1}$ . Introducing the ac susceptibility

$$\chi = \chi_0(\chi' - i\chi'') \quad (2)$$

the ac losses can be expressed as

$$W = \pi \chi'' \chi_0 \frac{B_0^2}{\mu_0} \quad (3)$$

where  $\chi''$  is the imaginary part of the ac susceptibility (called the internal susceptibility) and  $\chi_0$  is the external susceptibility under conditions of perfect screening, when the superconducting filaments are in the Meissner state. The magnitude of  $\chi_0$  represents the amplification of the applied field at the edge of the sample, due to surface screening currents. The internal susceptibility relates the sample magnetization to this effective field that the sample does really experience. For a long cylindrical sample in a parallel field  $\chi_0 \sim 1$ , the losses are therefore completely determined by  $\chi''$ , which can range from zero to 0.25. As the cylinder height reduces,  $\chi_0$  reaches values larger than unity. When the

cylinder approaches a thin disc, we find  $\chi_0 \gg 1$ . However, the change in shape does not affect the range of values of  $\chi''$ , which is related to the effective field. In the literature this topic has been largely discussed and analytical expressions have been found for regular shapes such as rectangular strips, wires and infinite arrays of strips [1–5]. For these cases the expressions of both  $\chi_0$  and  $\chi''$  exist.

When dealing with real multifilamentary tapes exposed to a perpendicular oscillating field, and although a significant literature does exist [6–8], several problems remain open.

- (i) Is equation (3) still applicable? Or, in other words, do the losses scale as  $\chi_0$  and according to some function  $\chi''(B)$ ?
- (ii) How can we evaluate  $\chi_0$ ?
- (iii) Which is the function  $\chi''(B)$ ?

This paper reports some attempts to answer these questions, through numerical and experimental approaches.

## 2. The superconducting tapes

In this paper we will refer to three particular tapes, shown in figure 1. They are BSSCO-based tapes with one or more superconducting cores inserted into a silver matrix: a monofilamentary tape with an elliptical cross section and two multifilamentary tapes with 19 and 36 filaments, manufactured by the Institute of Electrical Engineering of the Slovak Academy of Sciences [9, 10]. The process used for the construction of the tapes is the standard ‘powder-in-tube’ method. Precursor powder with a nominal composition of  $\text{Bi}_{0.6}\text{Pb}_{0.4}\text{Sr}_2\text{Ca}_2\text{Cu}_3\text{O}_x$  and pure Ag tubes, 7 mm in outer diameter and 5.5 mm in inner diameter, were used as starting materials. The multifilamentary tapes were fabricated by two deforming sequences. The first tape was built by 19 round wires inserted into a circular tube and the second one by 36 rectangular wires inserted into a rectangular tube. The critical current density  $J_C(B)$  at  $T = 77$  K for the tapes is shown in table 1, along with other relevant parameters.

## 3. External susceptibility

### 3.1. Calculation of $\chi_0$

Analytical expressions for  $\chi_0$  have been found by several authors [1–5] for samples with simple and regular shape, such as discs, tapes and infinite one-dimensional arrays of tapes. The analytical methods used to determine the external susceptibility are based on the Landau approach for a diamagnetic rotational ellipsoid in a perpendicular field [11]. The steps for finding  $\chi_0$  are:

- determination of the current density  $\vec{J}(\vec{r})$  and the field  $\vec{B}(\vec{r})$  on the surface of the sample, solving the Laplace equation;
- determination of the magnetic moment:

$$\vec{m} = (\mu_0/2) \int \vec{r} \times \vec{J}(\vec{r}) dV;$$

- determination of the magnetization:

$$\vec{M} = \vec{m}/V_{sample};$$

- determination of the external susceptibility:

$$\chi_0 = -M/B_0.$$

The main problem is that  $\vec{J}(\vec{r})$  and  $\vec{B}(\vec{r})$  can be analytically found only for the simple above-mentioned cases. In order to find  $\chi_0$  for structures more close to real tapes, we proposed in our previous paper [12] to involve numerical codes, such as ANSYS [13]. We used such an approach to obtain analytical expressions of the external susceptibility for regular shapes and numerical values of the external susceptibility in real tapes. The use of numerical codes allows us to calculate  $\chi_0$  in a more straightforward way; considering the energy variation  $\Delta W$  of a body with a given magnetization  $M$  placed in a field  $B$ ,  $\chi_0$  is given by [12]

$$\chi_0 = \frac{\Delta W}{(1/2\mu_0)B_0^2 V_{sample}} \quad (4)$$

where  $V_{sample}$  is the volume occupied by the magnetized body.  $\Delta W$  is calculated by starting from the field distribution in a region much larger than the sample.

We started considering the expressions for  $\chi_0$  found in the literature. Then we obtained empirical expressions for other regular shapes, such as finite arrays of tapes and two-dimensional regular matrices, by fitting the numerical results [12]. The final expressions of  $\chi_0$  are summarized in table 2. If a tape can be described as one of these systems, the theoretical value of  $\chi_0$  can be obtained using the formulae reported in this table. However, when the filament array in the tape is irregular, the only way to calculate the value of the external susceptibility is to use numerical codes. Figure 2 shows how the external field is shielded by the three tapes according to ANSYS calculations. The computed field distribution is used to evaluate  $\chi_0$  numerically.

### 3.2. Measurements and comparison with expectation

Provided that the sample volume is known, we can demonstrate that  $\chi_0$  is a physically measurable quantity. We use the experimental set-up based on the standard ac susceptometer [14] as shown in figure 3. An ac current flows in the primary coil of a transformer; it induces an ac field in two secondary pick-up coils: one containing the sample and the other remaining empty. There is also the possibility to superimpose a dc magnetic field using a superconducting magnet. All the coils are inserted into a cryostat with a variable temperature insert (VTI). If  $U_p$  is the voltage registered by the pick-up coil containing the sample and  $U_{coil}$  is that registered by the empty coil at the same time, the signal fed to the input of the lock-in amplifier is

$$U_{meas} = U_{coil} - U_p. \quad (5)$$

It is commonly known that the ac susceptibility components ( $\chi'$ ,  $\chi''$ ) are directly related to  $U_{meas}$  [15]. In the appendix we show that under particular conditions of complete sample shielding by Meissner currents—this is accomplished at low temperature and weak magnetic fields—the constant  $\chi_0$  can be determined as

$$\chi_0 = G_C \frac{V_{coil}}{V_{sample}} \frac{U_{meas}}{U_{coil}} \quad (6)$$

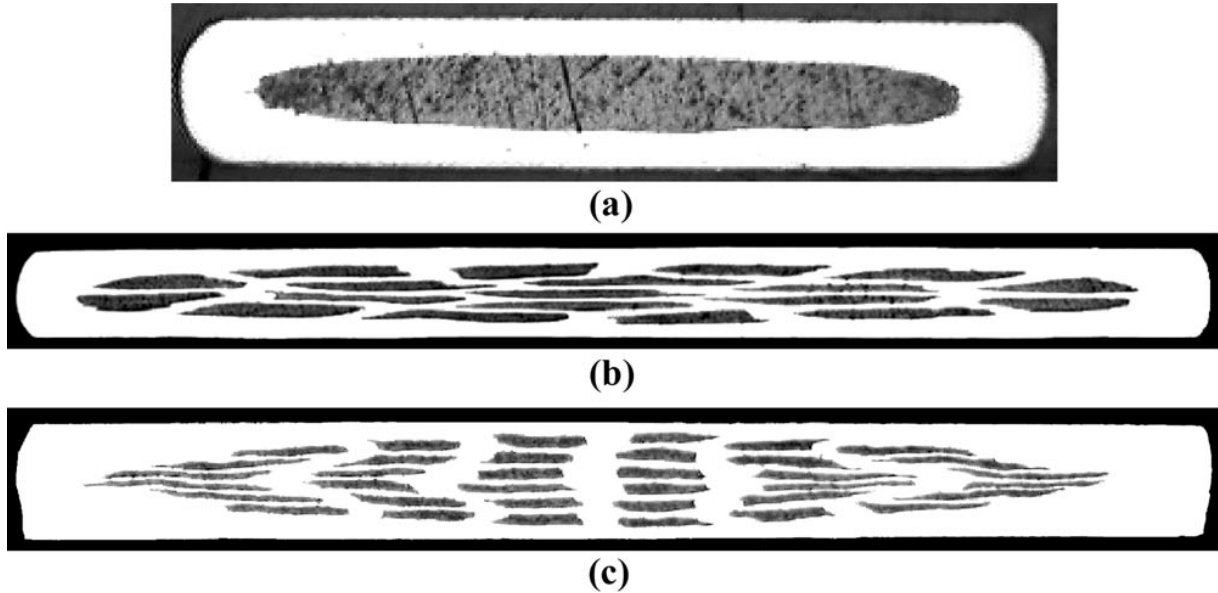


**Figure 1.** Cross sections of the monofilamentary tape (a), the 19-filament tape (b) and the 36-filament tape (c).

**Table 1.** The main characteristic of the three tapes.

	Monofilament tape	19-filament tape	36-filament tape
Tape width (mm)	1.80	2.50	2.50
Tape thickness (mm)	0.31	0.14	0.20
Average width $L$ of filaments (mm)	1.46	0.32	0.21
Average thickness $d$ of filaments ( $\mu\text{m}$ )	175	10	10
Superconducting cross section of the tapes ( $\text{m}^2$ )	$2.01 \times 10^{-7}$	$6.22 \times 10^{-8}$	$7.84 \times 10^{-8}$
$J_C$ at 77 K and no applied field ( $\text{A m}^{-2}$ )	$5.2 \times 10^7$	$1.0 \times 10^8$	$5.0 \times 10^7$

where  $V_{sample}$  is the sample volume,  $V_{coil}$  is the volume surrounded by the pick-up coil and  $G_C$  is a constant given by the pick-up coil shape.

The samples were pieces (7–8 mm) cut from the tapes mentioned in section 2. Numerical modelling has proved that under these conditions we can compare the experimental results with predictions obtained by two-dimensional analyses. The values of the external susceptibility obtained using a field of 0.1 mT and a frequency of 4.19 Hz are shown in table 3. It is important to mention that both the field amplitude and the frequency were low enough to guarantee that the field is shielded by the surface currents on each flat filament composing the tape. Table 3 also shows the values of  $\chi_0$  calculated for the single filaments and for the filamentary zone using the two-dimensional theoretical formulae for strips of rectangular and ellipsoidal cross sections. When making this comparison, it is extremely important to use the same value of  $V_{sample}$  for both previsions (equation (4)) and experimental results (equation (6)). For  $V_{sample}$  we used the volume occupied by the superconducting material only. The predictions and the experimental results compare very well, with deviations under 10%. In our previous paper [12], different values of  $\chi_0$  were computed for tapes (b) and (c). This apparent inconsistency is due to the use of a sample volume  $V_{sample}$  calculated considering the filaments of a rectangular cross section, rather than the real irregular shapes (see figure 1) as in the present paper.

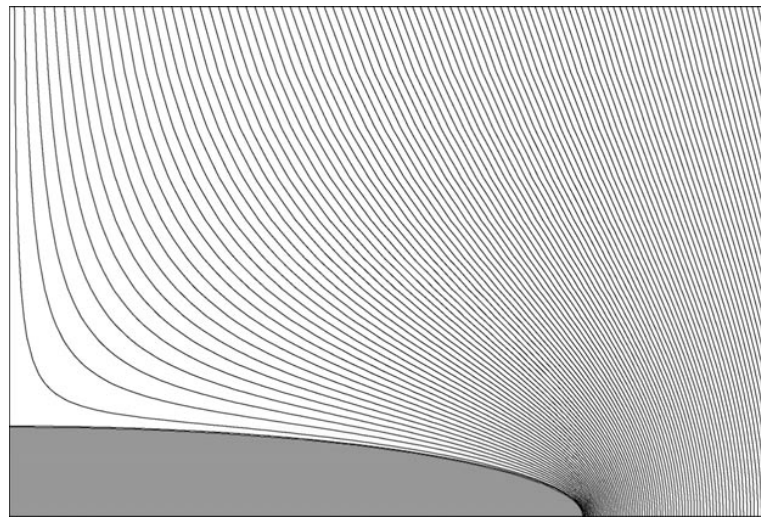
As remarked in the previous section, these values are much greater than one (especially for the 19-filament tape) and this shows the importance of knowing the external susceptibility, when the aim is to determine the losses. We can now give an answer to question (ii) of the introduction, stating that finite-element codes for magnetic analyses provide an excellent tool for computing the external susceptibility of any multifilamentary tape in a perpendicular field.

## 4. Internal susceptibility

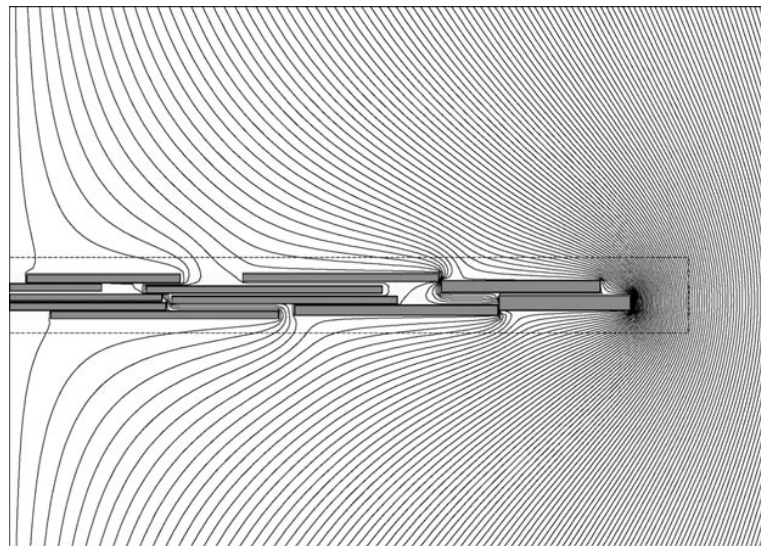
### 4.1. Calculation of $\chi''$

The main problem we face in the calculation of the internal susceptibility is that, at present, it cannot be computed with the same numerical method that was proved to work well for the external susceptibility in the Meissner state. This is because now the magnetic shielding is determined by bulk currents that lead to a magnetic hysteresis, according to the critical state model. Nevertheless interesting considerations come from the analytical solution of the problem found in the literature [1, 4, 5] for regular sample shapes, on the basis of the Norris approach [16]. The analytical method used to determine the internal susceptibility is based on the critical state model and consists of:

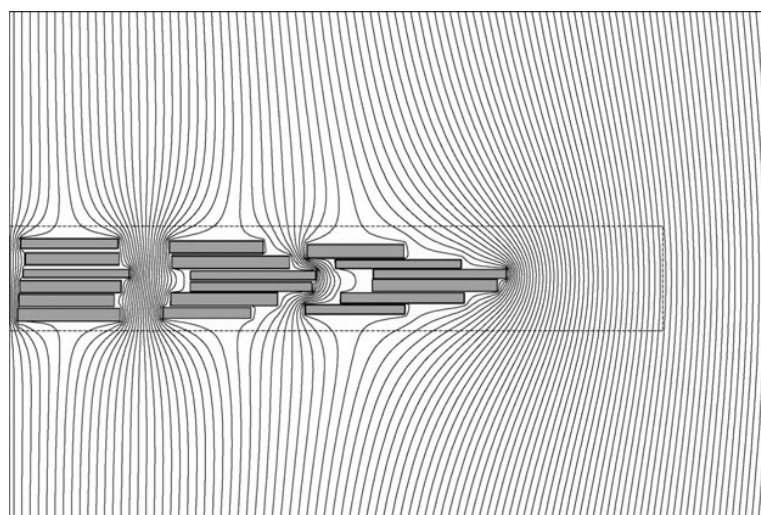
- determination of the current density  $\vec{J}(\vec{r})$  and the field  $\vec{B}(\vec{r})$  inside the sample using the critical state model;



(a)



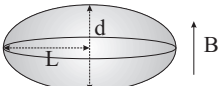
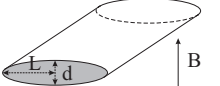
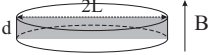
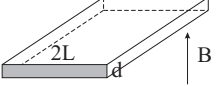
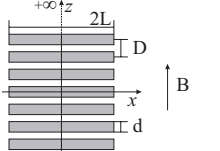
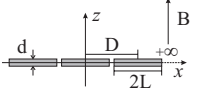
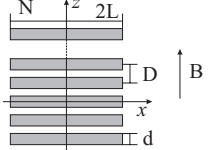
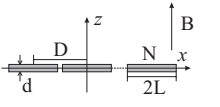
(b)



(c)

**Figure 2.** Flux lines for the monofilamentary tape (a), and those for the 19-filament tape (b) and the 36-filament tape (c).

**Table 2.** Expressions of  $\chi_0$ .

Sample geometry	External susceptibility
Rotational ellipsoid [1, 4] 	$\chi_0 = \frac{4L}{\pi d}$
Elliptical strip [1, 12] 	$\chi_0 = \frac{2\alpha L}{d}$ with $\alpha = [(1 + d/2L)/(1 - d/2L)]^{1/2}$
Disc [4] 	$\chi_0 = \frac{8}{3\pi} \frac{L}{d}$
Rectangular strip [1] 	$\chi_0 = \frac{\pi L}{2d}$
z stack [5] 	$\chi_{0,z-stack}(\infty) = \frac{D^2}{\pi L d} \ln \left[ \cosh \left( \frac{\pi L}{D} \right) \right]$ with $D$ as the distance between strips plus $d$
x array [5] 	$\chi_{0,x-array}(\infty) = -\frac{D^2}{\pi L d} \ln \left[ \cos \left( \frac{\pi L}{D} \right) \right]$ with $D$ as the distance between strips plus $2L$
Finite z stack [12] 	$\chi_0(N) = \chi_{0,z-stack}(\infty) + \frac{\chi_0(1) - \chi_{0,z-stack}(\infty)}{N^{0.8}}$ where $\chi_0(1) = \frac{\pi L}{2d}$
Finite x array [12] 	$\chi_0(N) = \chi_0(1) \left[ 1 + \frac{2}{\pi} (\beta - 1) \text{arcsec} \left( \frac{N + \Omega - 1}{\Omega} \right) \right]$ where $\beta = \frac{\chi_{0,x-array}(\infty)}{\chi_0(1)}$ and $\Omega = 5\beta$
xz matrix [12] ( $n_x \times n_z$ tapes) 	$\chi_0 = \frac{\pi L}{2d} \frac{f_x}{f_z}$ where $f_x = 1 + \frac{2}{\pi} (\beta - 1) \text{arcsec} \left( \frac{n_x + \Omega - 1}{\Omega} \right)$ $f_z = \chi_0(1) \left( \chi_0(\infty) + \frac{\chi_0(1) - \chi_{0,z-stack}(\infty)}{n_z^{0.8}} \right)^{-1}$

**Table 3.** Comparison between the experimental and the numerical values of the external susceptibility for the three tapes.

$\chi_0$	Monofilament tape	19-filament tape	36-filament tape
Experimental values	$8.9 \pm 0.4$	$68.7 \pm 2.6$	$13.7 \pm 0.8$
ANSYS values	9.6	64.2	14.9
As calculated from the elliptical strip model applied to single filaments	9.4	33.0	22.0
As calculated from rectangular strip model applied to single filaments	6.7	25.1	16.5
As calculated from elliptical strip model applied to a filament bundle	—	32.7	18.0
As calculated from rectangular strip model applied to a filament bundle	—	24.1	13.0

- determination of the magnetic moment,

$$\vec{m} = (\mu_0/2) \int \vec{r} \times \vec{J}(\vec{r}) dV;$$

- determination of the magnetization,

$$\vec{M} = \vec{m} / V_{sample};$$

- determination of the losses,

$$W = (1/\mu_0) \oint_{cycle} M dB;$$

- determination of the internal susceptibility,

$$\chi'' = \oint_{cycle} M dB / (\pi B_0^2 \chi_0).$$

When the sample is in the normal state or the shielding currents flow only along the surface (Meissner state), no bulk currents are present in the sample and  $\chi'' = 0$ . Between these two states  $\chi''$  has a maximum for a determined value of the external field, depending on the sample shape. It was found that the model of an infinitely thin strip or disc in a perpendicular magnetic field best fits the experimental results obtained on stand-alone multifilamentary tapes in this field

**Table 4.** Analytical expressions of the internal susceptibility for simple shapes.

Sample	Expression of $\chi''$
Strip [1]	$\chi''_{strip} \left( \frac{B_0}{B_c} \right) = \frac{4}{\pi} \frac{B_c}{B_0} g \left( \frac{B_0}{B_c} \right)$ where $g(x) = \frac{2}{x} \ln(\cosh x) - \tanh x$
z stack [5]	$\chi''_{stack} \left( \frac{B_0}{B_c} \right) = \frac{2}{\pi} \left( \frac{B_c}{B_0} \right)^2 \frac{1}{\ln[\cosh(\pi L/D)]} \tilde{I}_{stack}$ where $\tilde{I}_{stack} = \int_0^{B_0/B_c} d \left( \frac{B}{B_c} \right) \left[ \left( \frac{B_0 - 2B}{B_c} \right) \ln \left( 1 + \frac{\sinh^2(\pi L/D)}{\cosh^2(B/B_c)} \right) \right]$
x array [5]	$\chi''_{array} \left( \frac{B_0}{B_c} \right) = \frac{2}{\pi} \left( \frac{B_c}{B_0} \right)^2 \frac{1}{\ln[\cos(\pi L/D)]} \tilde{I}_{array}$ where $\tilde{I}_{array} = \int_0^{B_0/B_c} d \left( \frac{B}{B_c} \right) \left[ \left( \frac{B_0 - 2B}{B_c} \right) \ln \left( 1 + \frac{\sin^2(\pi L/D)}{\cos^2(B/B_c)} \right) \right]$
Disc [4]	$\chi''_{disc} \left( \frac{B_0}{B_c} \right) = \frac{2}{\pi} \int_0^\pi \left\{ -S \left( \frac{B_0}{B_c} \right) + (1 - \cos \vartheta) S \left[ \frac{1}{2} \left( \frac{B_0}{B_c} \right) (1 - \cos \vartheta) \right] \right\} \sin \vartheta d\vartheta$ where $S(x) = \frac{1}{2x} \left[ \cos^{-1} \left( \frac{1}{\cosh x} \right) + \frac{\sinh x}{\cosh^2 x} \right]$

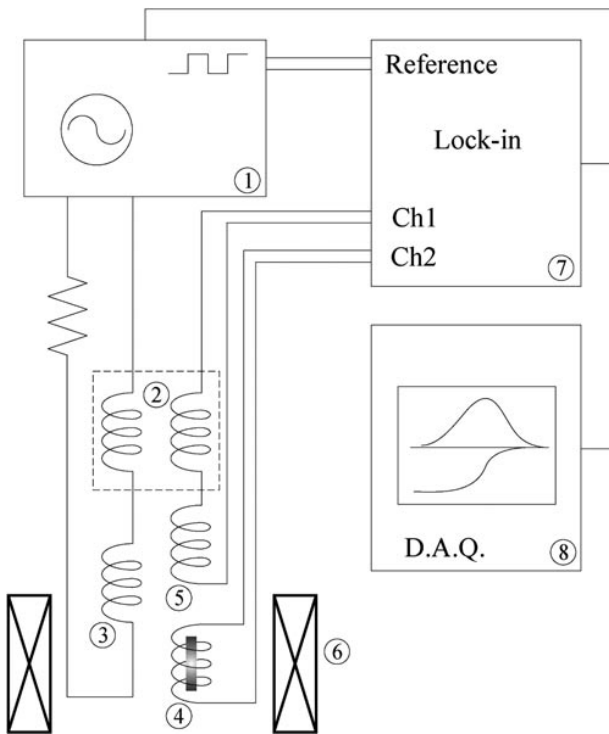


**Figure 3.** Arrangement of the experimental setup: (1) signals generator, (2) signal adapter (a transformer), (3) primary coil, (4) pick-up coil containing the sample, (5) empty pick-up coil, (6) dc coil, (7) lock-in analyser and (8) controller.

geometry [17]. Then

$$\chi''_{max} = \begin{cases} 0.234 \text{ at } B = B_{max} = 2.465 B_c & \text{for strips} \\ 0.240 \text{ at } B = B_{max} = 1.944 B_c & \text{for discs} \end{cases} \quad (7)$$

where  $B_c$  is the characteristic field, defined as

$$B_c = \begin{cases} \frac{\mu_0 J_C d}{\pi} & \text{for strips} \\ \frac{\mu_0 J_C d}{2} & \text{for discs} \end{cases} \quad (8)$$

where  $d$  is the thickness of the strip or of the disc. All the analytical expressions for simple systems are summarized in table 4 and plotted in figure 4. These expressions all depend on  $B_0/B_c$ . It is worth mentioning that, as shown

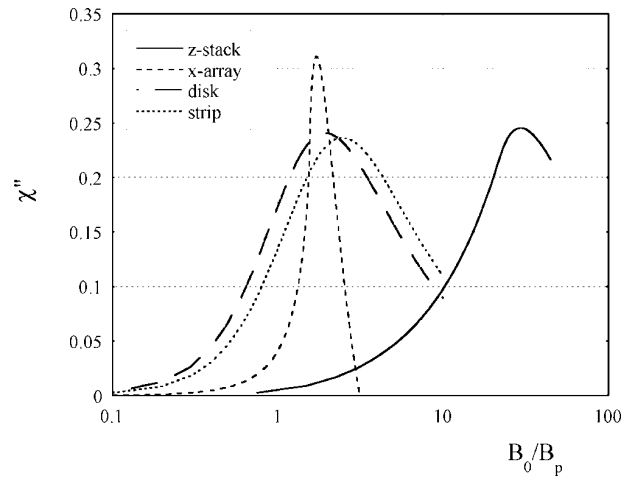


**Figure 4.** Theoretical profiles of  $\chi''$  according to the basic theories for simple and regular shapes.

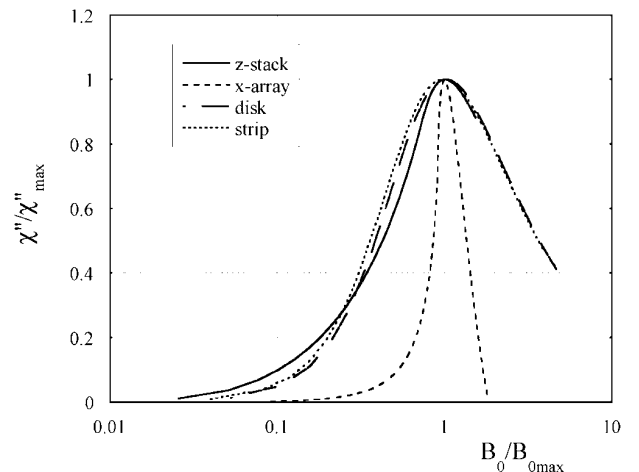


**Figure 5.** Theoretical profiles of  $\chi''$  normalized to their maximum values.

in figure 5, normalizing the imaginary part of the complex ac susceptibility to its maximum value  $\chi''_{max}$ , at the field  $B_{0max}$ , and plotting the normalized value  $\chi''/\chi''_{max}$  against the normalized field  $B_0/B_{0max}$ , we obtain very similar curves for discs, strips and, surprisingly, for an infinite z stack of strips as well. Let us now compare these models with the experimental results.

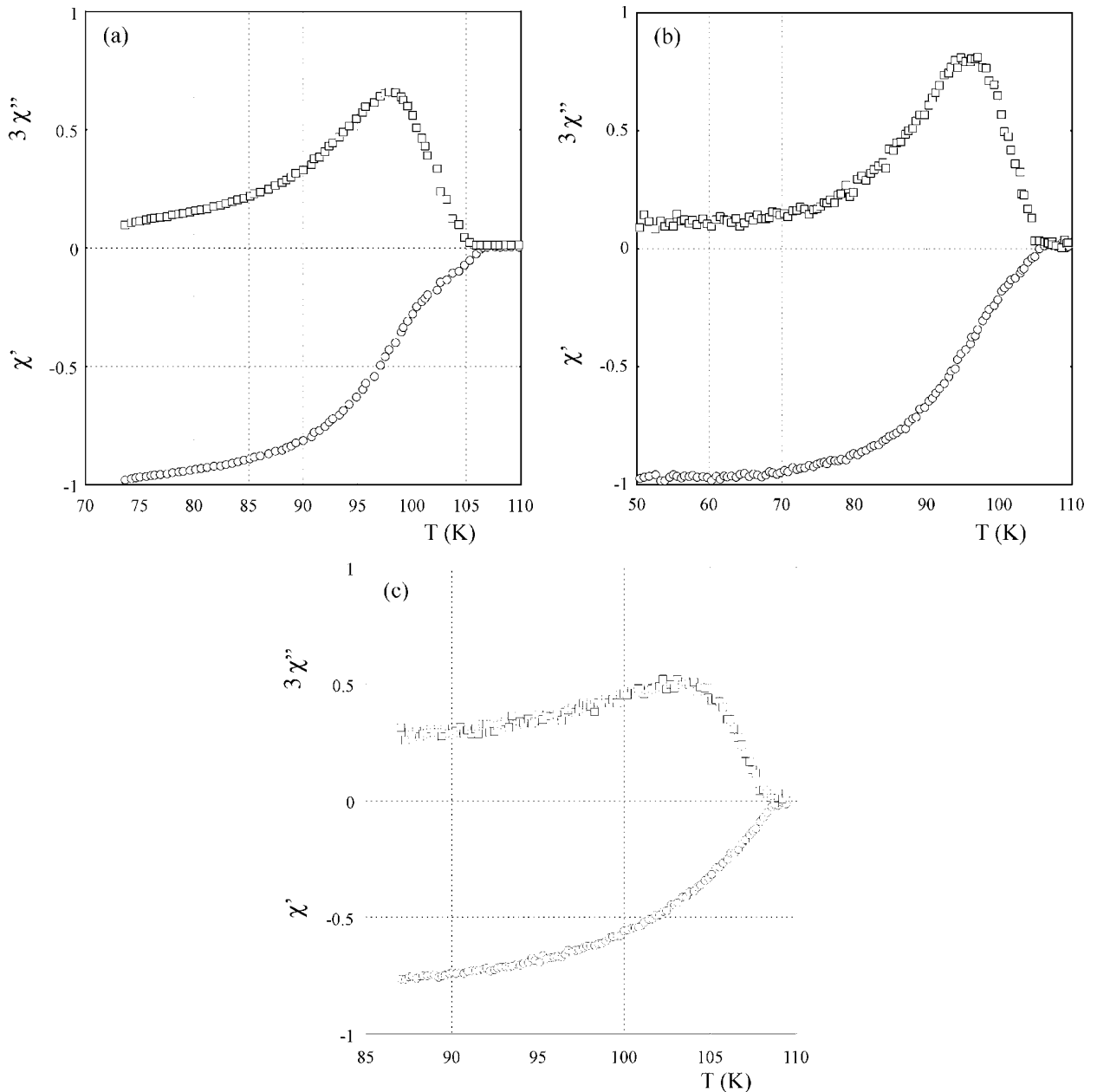


**Figure 6.**  $\chi''(T)$  at  $B_0 = 1.2$  mT and a frequency of 4.19 Hz for the monofilament tape (a), at  $B_0 = 0.15$  mT and a frequency of 3.5 Hz for the 19-filament tape (b) and at  $B_0 = 0.05$  mT and a frequency of 140 Hz for the 36-filament tape (c).

#### 4.2. Measurements and comparison with expectation

The arrangement to determine the internal susceptibility is the same as we used to test the external susceptibility, as reported in section 3.2. Remember that the lock-in amplifier allows us to separate the first harmonic from the pick-up coil's signal, and to determine the real and imaginary parts with respect to a reference signal. We identified the real axis of a complex plane with the purely inductive signal taken from the empty pick-up coil. Thus the real channel output of the lock-in amplifier is proportional to  $\chi'$ , while the imaginary one to  $\chi''$ . The proportionality constant, necessary to convert the lock-in outputs to the internal susceptibility parts, is derived assuming that the real part should range from zero, in the normal state, to  $-1$ , in the

Meissner state. This procedure is equivalent to establishing the internal susceptibility by dividing the measured external susceptibility by  $\chi_0$ .

Figure 6 shows how the real and imaginary parts of the internal ac susceptibility for the three samples depend on the temperature for different values of the frequency and peak ac fields. The measured maximum value of  $\chi''$  is  $0.23 \pm 0.01$  for the monofilament tape,  $0.25 \pm 0.01$  for the 19-filament tape and  $0.174 \pm 0.025$  for the 36-filament tape. These values can be compared with the expectations of theories for a single strip or disc, predicting a maximum around 0.23–0.24. The facts that multifilamentary tapes display behaviour of  $\chi''(T)$  similar to those of the single strip or disc and that the maximum of the susceptibility ranges from  $0.17\chi_0$  to  $0.25\chi_0$  lead to two important considerations:

**Table 5.** Experimental values of  $B_{0max}$  and the effective thickness  $d$  for the monofilament tape.

Temperature (K)	$B_{0max}$ (mT)	$J_C$ ( $A\ m^{-2}$ )	$d$ (m)	
			Strip theory	Disc theory
$50 \pm 1$	$30.4 \pm 1$	$11.8 \times 10^7$	$2.6 \times 10^{-4}$	$2.1 \times 10^{-4}$
$60 \pm 1$	$21.9 \pm 1$	$9.3 \times 10^7$	$2.4 \times 10^{-4}$	$1.9 \times 10^{-4}$
$70 \pm 1$	$12.3 \pm 1$	$7.0 \times 10^7$	$1.8 \times 10^{-4}$	$1.4 \times 10^{-4}$

**Table 6.** Experimental values of  $B_{0max}$  and the effective thickness  $d$  for the 19-filament tape.

Temperature (K)	$B_{0max}$ (mT)	$J_C$ ( $A\ m^{-2}$ )	$d$ (m)	
			Strip theory	Disc theory
$60 \pm 1$	$1.9 \pm 1$	$1.9 \times 10^8$	$1.0 \times 10^{-5}$	$0.8 \times 10^{-5}$
$70 \pm 1$	$1.3 \pm 1$	$1.4 \times 10^8$	$0.9 \times 10^{-5}$	$0.8 \times 10^{-5}$
$80 \pm 1$	$0.7 \pm 1$	$0.9 \times 10^8$	$0.8 \times 10^{-5}$	$0.7 \times 10^{-5}$

**Table 7.** Experimental values of  $B_{0max}$  and the effective thickness  $d$  for the 36-filament tape.

Temperature (K)	$B_{0max}$ (mT)	$J_C$ ( $A\ m^{-2}$ )	$d$ (m)	
			Strip theory	Disc theory
$60 \pm 1$	$2.5 \pm 1$	$9.7 \times 10^7$	$2.6 \times 10^{-5}$	$2.1 \times 10^{-5}$
$70 \pm 1$	$1.7 \pm 1$	$7.3 \times 10^7$	$2.3 \times 10^{-5}$	$1.8 \times 10^{-5}$
$80 \pm 1$	$1.1 \pm 1$	$4.7 \times 10^7$	$2.4 \times 10^{-5}$	$1.9 \times 10^{-5}$
$90 \pm 1$	$0.6 \pm 1$	$2.0 \times 10^7$	$3.0 \times 10^{-5}$	$2.4 \times 10^{-5}$

- although we do not have a specific theory for the critical state of multifilamentary tapes in a perpendicular field, we can try to apply the theories developed for a single strip or disc;
- the ac losses scale with  $\chi_0$ , answering positively to question (i) proposed in the introducing remarks of this paper.

We can try now to give an answer to the third question posed at the beginning, i.e. that is the behaviour of  $\chi''(B)$  for multifilamentary tapes. We can take advantage of the previous results, indicating that the theories for a single strip and disc can also be used for multi-strips. Following this line of enquiry, we measured  $\chi''$  as a function of the applied peak field  $B_0$ . Figure 7 shows  $\chi''(B_0)$  for the monofilamentary tape at three different temperatures. We obtained maxima of  $\chi''$  around 0.23–0.24 at the field of 30.4 mT at 50 K, 21.9 mT at 60 K and 12.3 mT at 70 K. At this point, knowledge of the critical current density determined independently in a transport experiment is crucial. Only then, can one extract the thickness of the superconducting element (disc, strip) observed in magnetic measurements from the susceptibility data. Let us consider, as an example, one of this data, i.e. that at 70 K. Since the critical current density in a monofilamentary set tape is  $J_C(T = 70\text{ K}, B = 0) = 6.16 \times 10^7\text{ A m}^{-2}$ , we can compute both the characteristic field and the effective strip thickness using equations (7) and (8). Applying the theory for strips we find  $B_c(T = 70\text{ K}) = 5.0\text{ mT}$  and  $d = 1.4 \times 10^{-4}\text{ m}$ . We can also apply the theory developed for discs, finding  $B_c(T = 70\text{ K}) = 6.3\text{ mT}$  and  $d = 1.63 \times 10^{-4}\text{ m}$ . Table 5 shows the calculated effective thickness for the monofilament type as extracted from all the measurements. Tables 6

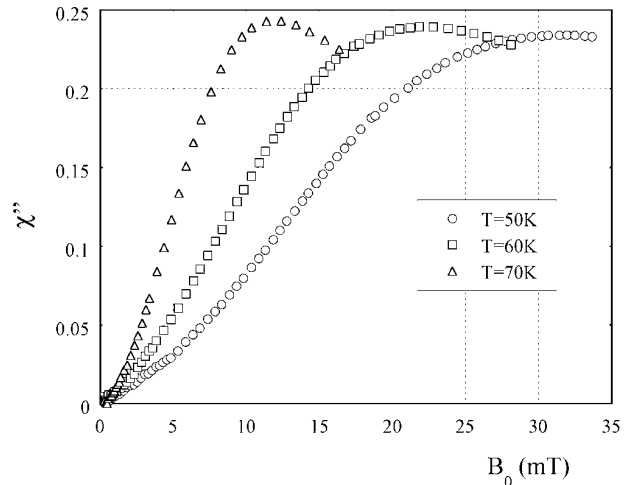


**Figure 7.**  $\chi''(B_0)$  for the monofilament tape at three different temperatures.

and 7 show the results obtained on multifilamentary tapes.

Considering both the strip and disc theory and considering all the data, the effective thickness  $d$  of the monofilament tape ranges from 140 to 260  $\mu\text{m}$ . These values compare well with the real filament thickness of 175  $\mu\text{m}$  (as shown in table 1). In the same way we find for the 19-filament tape  $6.5\ \mu\text{m} < d < 10\ \mu\text{m}$ . Averaging these values we have  $d = 8.3\ \mu\text{m}$  (10  $\mu\text{m}$  is the real average thickness of the filaments). For the 36-filament tape  $18\ \mu\text{m} < d < 30\ \mu\text{m}$  for an average value of  $d = 24\ \mu\text{m}$  (10  $\mu\text{m}$  is the real average thickness). These results allow us to draw two important conclusions: first, the internal susceptibility

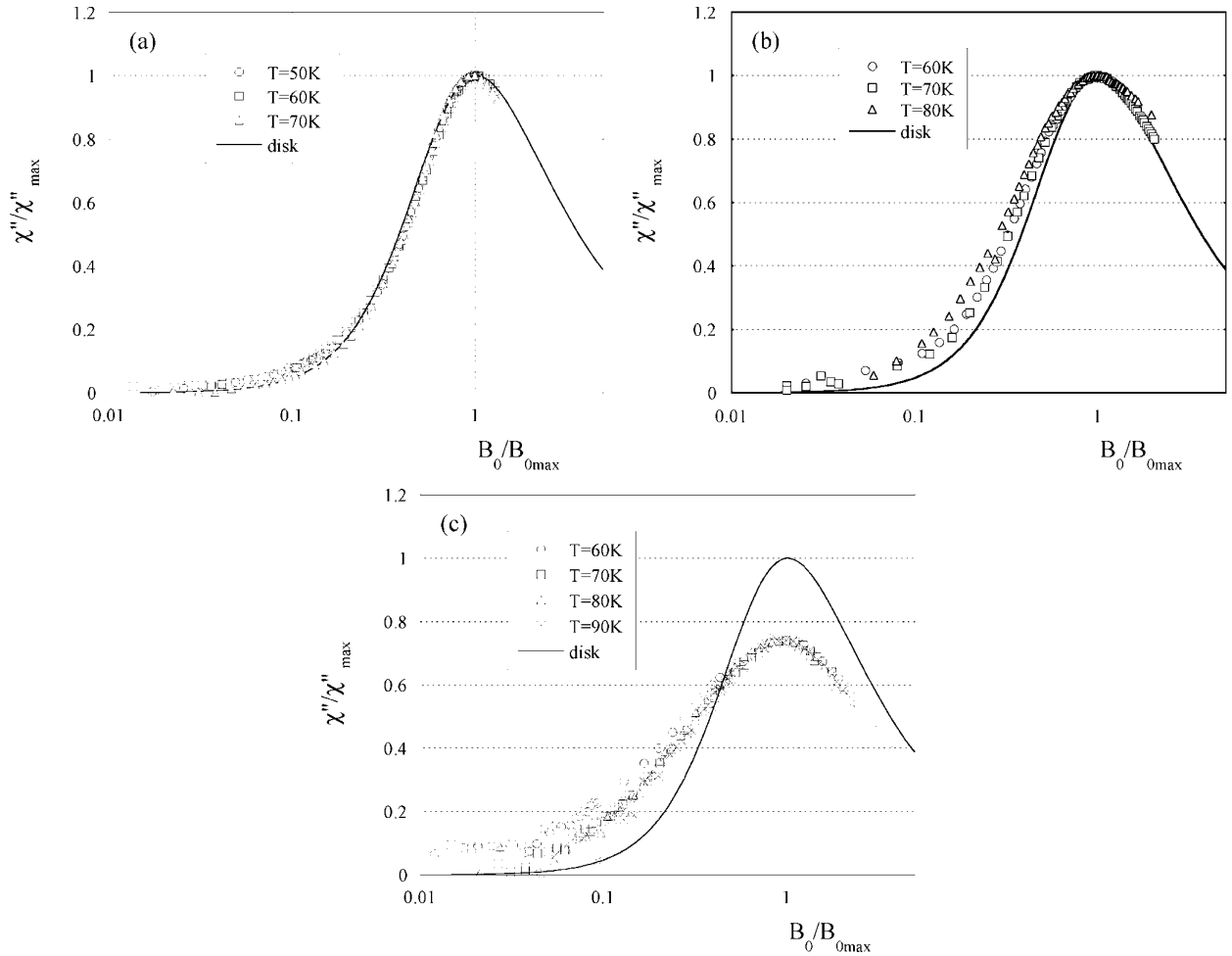


**Figure 8.** Normalized curves  $\chi''/\chi''_{max}$  for the monofilament (a), 19-filament tape (b) and 36-filament tape (c). The curve for the 36-filament tape has been normalized to  $\chi''_{max} = 0.234$ .

reflects the field penetration into a single filament, rather than the whole filamentary zone. Then, in the case of a columnar arrangement, the currents in individual filaments are correlated, leading to an apparent increase of the filament thickness.

As last step we have analysed how the normalized internal susceptibility  $\chi''/\chi''_{max}$  scales with the normalized field  $B_0/B_{0max}$ ; the results are shown in figure 8 for the three tapes, together with the theoretical curve calculated for a disc, and include the following.

- For the monofilament tape we find that the data measured at the three different temperatures lay on the theoretical curve. This means that a wide band of shielding current distributions is described by the disc (or strip) theory.
- For the 19-filament tape the agreement is still fair, but deviations occur at low penetrations, indicating that the filamentary structure is not perfectly homogeneous. Varying filament thickness is observable in the micrograph of the tape; further distortions in the current distribution with respect to a single-filament model could be caused by the different electrical properties of the individual filaments.

- For the 36-filament tape, the data measured at four temperatures again fall on a common curve, indicating that the current distribution follows the same pattern at different absolute values of the critical current density. However, after dividing by the theoretical  $\chi''_{max} = 0.234$ , the peak does not reach one. Moreover, we clearly see that now the shape of the curve is changed from the theoretical curve.

Apart from the results on the monofilament tape, clearly showing that the theories for a single strip or disc are capable of describing the field penetration transversally to a tape, we focused our attention on the multifilamentary tapes, showing deviations from single disc or strip theories. We can explain this behaviour by considering that the single filaments composing the tapes do not have the same electrical properties, i.e. the critical current density can, in principle, be different for each filament [19]. As a result, the ratio  $x = B_0/B_c$  may be different for each filament in the tape. We can generalize this situation stating that the ac losses in a multifilamentary tape in a perpendicular field of peak amplitude  $B_0$  are given by the sum of the ac losses in each filament. Using one of the existing models (strip) we can

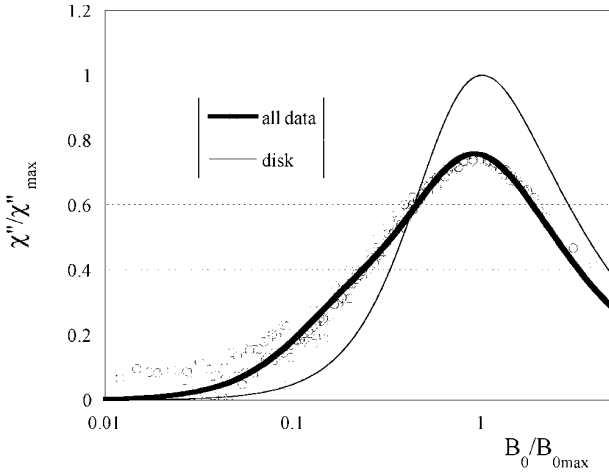


**Figure 9.** Fit of the 36-filament tape data using a convolution of functions.

write the internal susceptibility as

$$\chi'' = \frac{1}{N} \sum_{i=1}^N \frac{4}{\pi} \frac{1}{x_i} \left( \frac{2}{x_i} \ln(\cosh x_i) - \tanh x_i \right) \quad (9)$$

where  $x_i$  is the effective applied field to characteristic field ratio for the filament  $i$ . Although we are not able to give an explicit expression of equation (9) for the two multifilamentary tapes under study, we can show that it is possible to fit the experimental data using a simplified version of equation (9). In particular figure 9 shows a fit of the data for the 36-filament tape summing only two functions: for 70% of the strips the characteristic field is  $B_{c1} = 0.95 B_c$  and for the remaining 30%  $B_{c2} = 4.28 B_c$ . As a result of the overlapping, the peak is broader and the maximum value of  $\chi''$  does not reach its theoretical value.

## 5. Conclusions

We have addressed the problem of calculating the ac losses for a multifilamentary superconducting tape placed in an oscillating perpendicular magnetic field. The main conclusions are the following.

- The ac losses are given by equation (3). Thus, to evaluate the losses, we need to know the imaginary part of the internal susceptibility  $\chi''(B_0)$  as well as the value of the external ac susceptibility at perfect shielding,  $\chi_0$ .
- The external susceptibility at perfect shielding can be computed using a suitable finite-element code for magnetic analysis.
- The internal susceptibility can be computed by applying existing models for a single strip or disc to the single filaments of the tape. Deviations may exist due to inhomogeneity of the transport critical current (between filaments) and/or peculiar filament distribution.
- The general problem to find a critical state model for finite array of strips still remains open. When the deviations to the internal susceptibility were given only to  $J_C$  inhomogeneity, the single strip and disc models can account completely for ac losses.

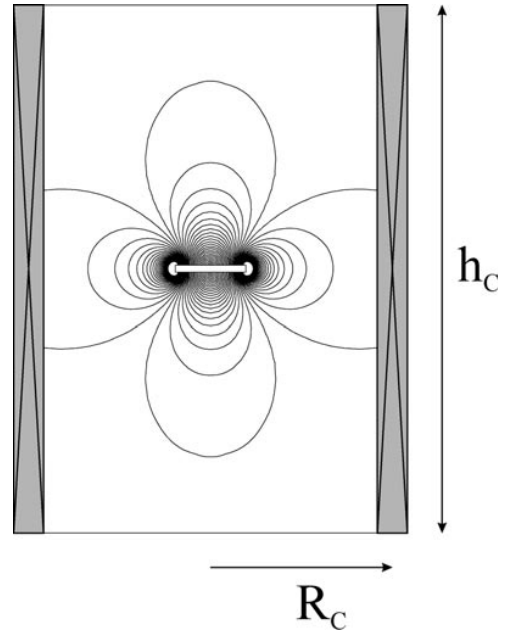


**Figure 10.** Magnetic dipole in the centre of a thin cylindrical coil with a radius  $R_C$  and height  $h_C$ .

## Appendix

To estimate the signal that a flat superconducting sample in the Meissner state produces in a cylindrical coil, we used the following approximation (see figure 10). The sample is represented by a magnetic dipole  $\vec{m}$ , oriented parallel with the pick-up coil axis. The vector potential, generated by such an object, has, in cylindrical coordinates, only the circumferential component [18]

$$A_\theta(z, r) = \frac{m r}{4\pi (r^2 + z^2)^{3/2}}. \quad (A.1)$$

We neglect the radial thickness of the pick-up coil winding, defining its shape by the radius  $R_C$  and height  $h_C$ . It has  $N_C$  turns, wound with constant density  $N_C/h_C$ . The magnetic flux created by the sample and linked to the turn with coordinate  $z$  is found by Stokes's theorem as

$$\phi(z) = 2\pi R_C A_\theta(z, R_C) = \pi R_C^2 \frac{m}{2\pi (R_C^2 + z^2)^{3/2}}. \quad (A.2)$$

The total magnetic flux linked with the pick-up coil is then

$$\psi = \frac{N_C}{h_C} \int_{-h_C/2}^{h_C/2} \phi(z) dz = \frac{N_C}{h_C} \frac{m}{G_C} \quad (A.3)$$

where we introduced an auxiliary constant given by the pick-up coil shape:

$$G_C = \left[ 1 + \left( \frac{2R_C}{h_C} \right)^2 \right]^{1/2}. \quad (A.4)$$

Now we include in our considerations the existence of the second, empty pick-up coil, with the same characteristics, placed at an axial distance large enough to neglect the magnetic flux generated by the sample. However, the driving field  $B(t) = B_0 \cos \omega t$  is supposed to be homogeneous in a

space scale much larger than the dimensions of the pick-up coil system. Thus, the signal induced in the empty pick-up coil will be

$$U_{coil} = -N_C \pi R_C^2 \frac{\partial B}{\partial t} = \frac{N_C}{h_C} V_{coil} \omega B_0 \quad (\text{A.5})$$

where the coil volume is  $V_{coil} = \pi R_C^2 h_C$ . For the pick-up coil containing the sample, on top of the signal induced by the driving field, there is the voltage due to the magnetic flux generated by the sample and given by equation (A.3). Being in the Meissner state, the magnetic moment of the sample will vary as

$$m(t) = -m_a \cos \omega t \quad (\text{A.6})$$

with  $m_a > 0$ . Thus, the voltage induced in the pick-up coil containing the sample, considering equation (A.3) and (A.6), will be

$$U_p = \frac{N_C}{h_C} \omega V_{coil} B_0 - \frac{N_C}{h_C} \omega \frac{1}{G_C} m_a \quad (\text{A.7})$$

and the resulting signal fed to the lock-in input is found from equations (A.5) and (A.7) as

$$U_{meas} = U_{coil} - U_p = \frac{N_C}{h_C} \omega \frac{m_a}{G_C} \quad (\text{A.8})$$

which, with the help of equation (A.5), can be rewritten as

$$m_a = \frac{U_{meas}}{U_{coil}} V_{coil} B_0 G_C. \quad (\text{A.9})$$

Taking into account the definition of magnetization as the volume density of the dipole moment, we find that

$$\chi_0 = \frac{-M_{Meiss}}{B_0} = \frac{m_a}{V_{sample}} \frac{1}{B_0}. \quad (\text{A.10})$$

Inserting equation (A.9) in this expression we finally obtain

$$\chi_0 = G_C \frac{U_{meas}}{U_{coil}} \frac{V_{coil}}{V_{sample}}. \quad (\text{A.11})$$

## References

- [1] Brandt E H 1994 *Phys. Rev. B* **49** 9355
- [2] Brandt E H 1998 *Phys. Rev. B* **58** 6506
- [3] Brandt E H 1998 *Phys. Rev. B* **58** 6523
- [4] Clem J R and Sanchez A 1994 *Phys. Rev. B* **50** 9355
- [5] Mawatari Y 1996 *Phys. Rev. B* **54** 13 215
- [6] Kwasnitza K, Clerc St, Flukiger R and Huang Y B 1998 *Physica C* **299** 113
- [7] Chiba T, Li Q, Ashworth S P, Suenaga M and Haldar P 1999 *IEEE Trans. Appl. Supercond.* **9** 2143
- [8] Oomen M P, Rieger J, Leghissa M and ten Kate H H J 1997 *Physica C* **290** 281
- [9] Kováč P, Husek I and Kopera L 1997 *Supercond. Sci. Technol.* **10** 982
- [10] Kováč P, Husek I, Rosova A and Pachla W 1999 *Physica C* **312** 179
- [11] Landau L D and Lifshitz E M 1982 *Electrodynamics of continuous media Theoretical Physics* vol 8 (Moscow: Nauka)
- [12] Fabbriatore P, Farinon S, Innocenti S and Gömöry F 2000 *Phys. Rev. B* **61** 6413
- [13] Swanson Analysis Systems Inc 2000 *Computer Code ANSYS* revision 5.6
- [14] Fabbriatore P, Farinon S, Gemme G, Musenich R, Parodi R and Zhang B 1993 *Cryogenics* **33** 1170
- [15] Gömöry F 1997 *Supercond. Sci. Technol.* **10** 523
- [16] Norris W T 1970 *J. Phys. D: Appl. Phys.* **3** 489
- [17] Gömöry F, Gherardi L, Crotti G, Bettinelli D, Martini L, Bigoni L and Zannella S 1998 *Physica C* **310** 168
- [18] Jackson J D 1962 *Classical Electrodynamics* (New York: Wiley)
- [19] Schuster T, Kuhn H, Weisshardt A and Kronmueller H 1996 *Appl. Phys. Lett.* **69** 1954